Supplementary Data for

CDH3-Directed Immunotherapy Targets Basal-like Hormone Receptor Negative Prostate Cancer and Breast Cancer

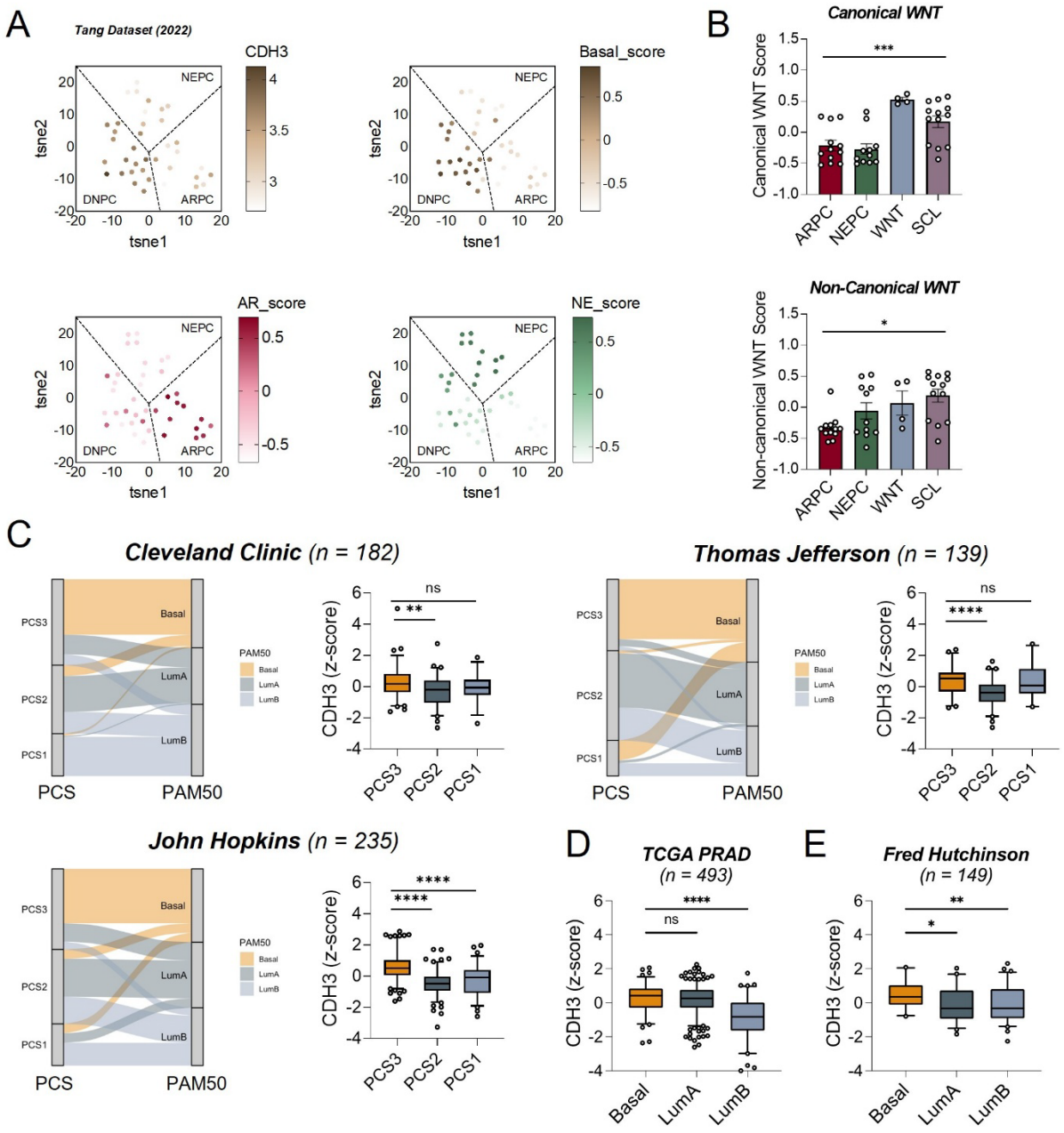
Guoqiang Liu et al.

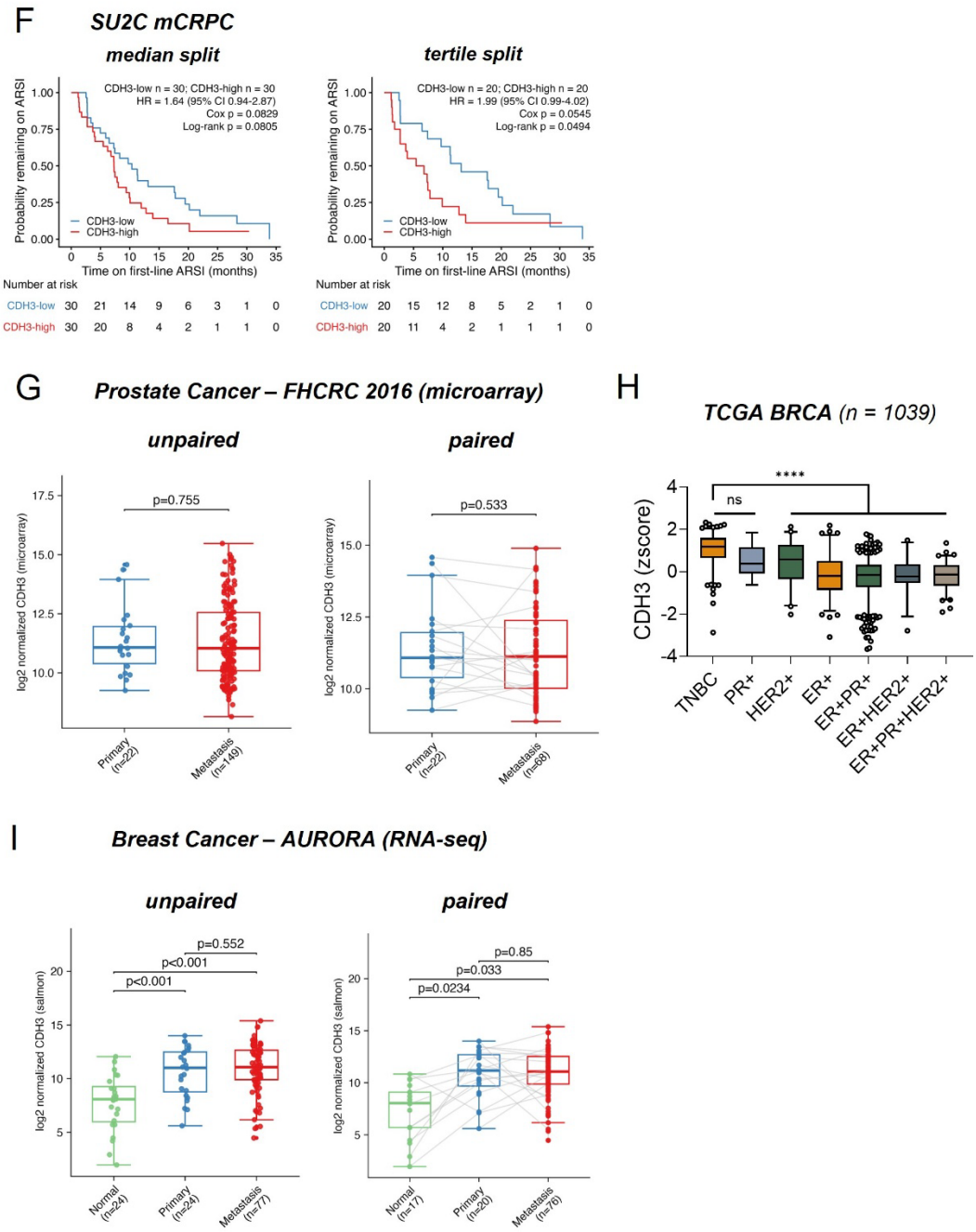
This PDF file includes:

Figures S1 to S7

Tables S1 to S3

Figure S1. High CDH3 expression in human basal-like prostate cancer and breast cancer.



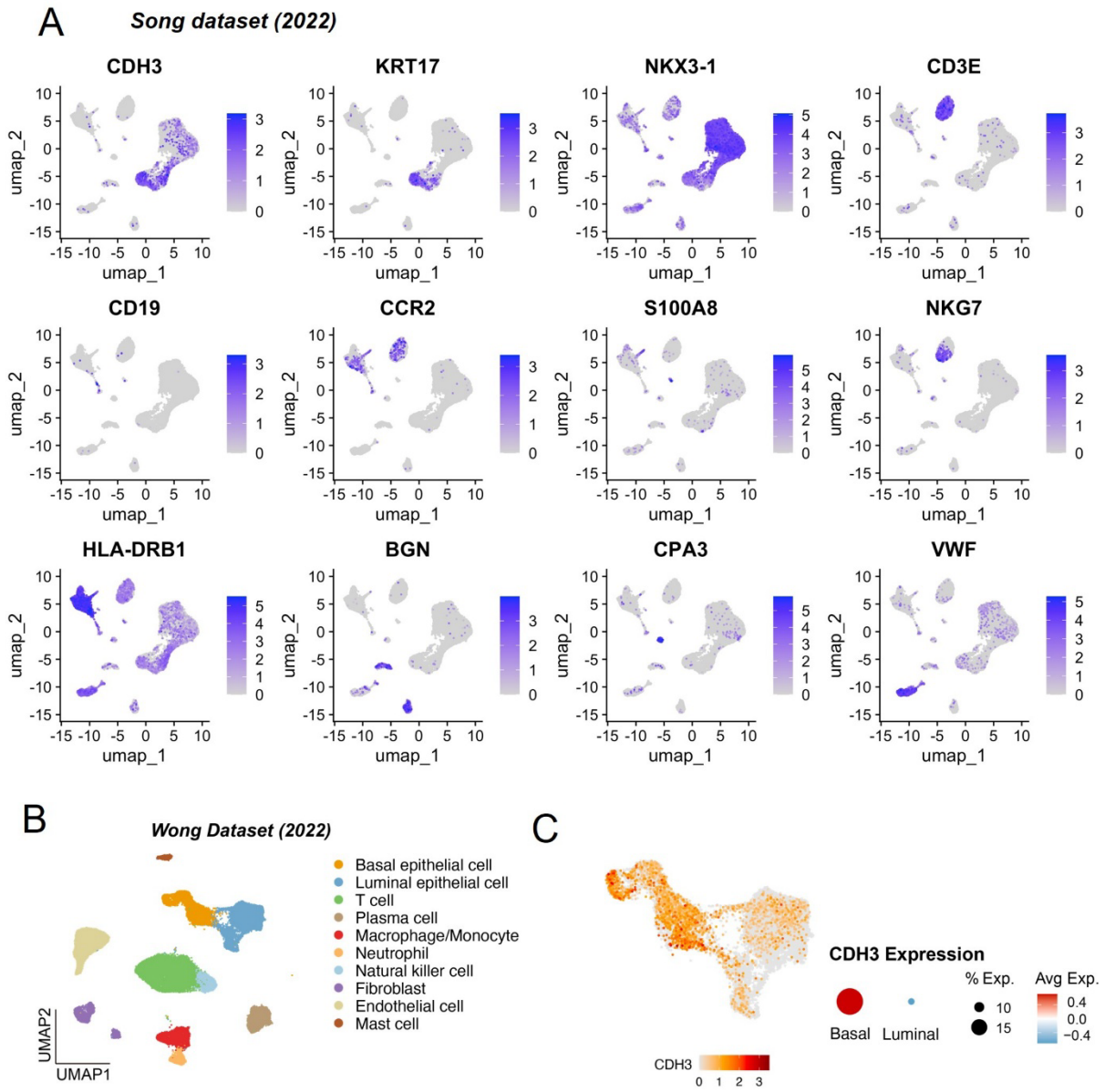


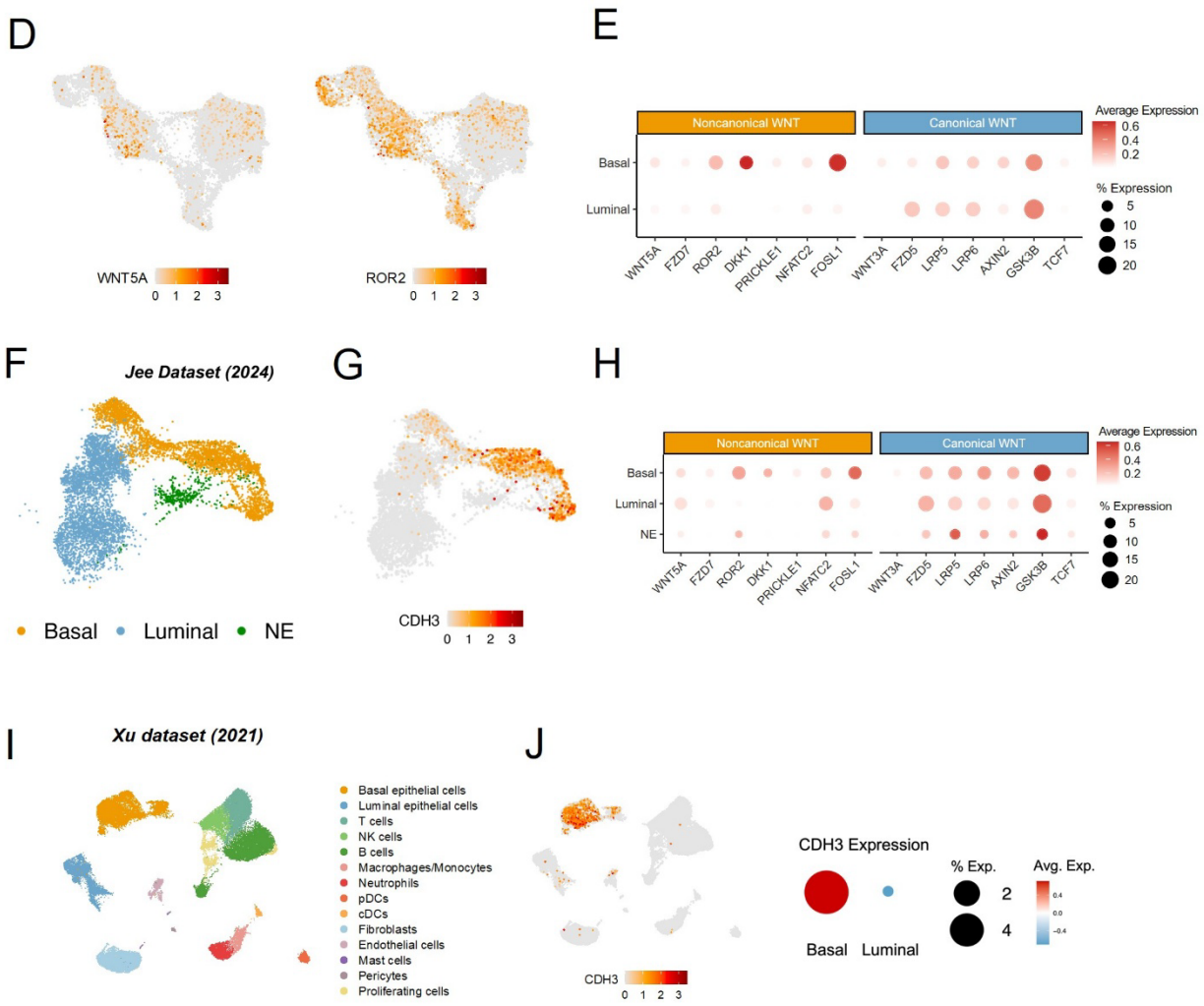
(A) t-SNE plots of Tang et al. (2022) human PCa models colored based on *CDH3* expression or different gene signature scores (AR, NE, basal). **(B)** Canonical and non-canonical WNT signaling scores for the four groups of human PCa models in Tang et al. **(C)** Patient classification by PCS or PAM50 method from three human PCa cohorts, Cleveland Clinic, Thomas Jefferson University, and Johns Hopkins University (left panels), and box plots showing

CDH3 expression across three PCS-based subtypes (right panels). **(D)** *CDH3* expression levels in the three PAM50-based subtypes of the TCGA PRAD cohort. **(E)** *CDH3* expression levels in the three PAM50-based subtypes of the metastatic PCa cohort from Fred Hutchinson Cancer Research Center. **(F)** Kaplan–Meier analysis of time on androgen receptor signaling inhibitor (ARSI) therapy in the SU2C mCRPC cohort, with patients stratified into CDH3-high and CDH3-low groups by either the cohort median or upper and lower expression tertiles. **(G)** *CDH3* expression in primary and metastatic PCa specimens from the FHCRC 2016 transcriptomics cohort, shown as unpaired (left) and matched patient-level (right) comparisons. **(H)** *CDH3* expression levels in subtypes defined by ER/PR/HER2 biomarkers in the TCGA BRCA cohort. **(I)** *CDH3* expression in normal breast tissue, primary breast tumors, and metastatic breast tumors from the AURORA RNA-seq cohort, shown as unpaired (left) and matched patient-level (right) comparisons.

Error bars represent SEM. Boxes span the 25th to 75th percentiles with the horizontal line indicating the median, whiskers extend to the 5th and 95th percentiles, and only data points outside the whiskers are shown. Kruskal–Wallis test (non-parametric ANOVA) for **(B)** and Dunn's multiple-comparisons test (rank-based; Kruskal–Wallis framework) for **(C)–(E)** and **(H)**. In **(F)**, hazard ratios and 95% confidence intervals were estimated using Cox proportional hazards regression, and groups were compared by log-rank test. For **(G)** and **(I)**, unpaired comparisons were performed using Wilcoxon rank-sum tests and paired comparisons using Wilcoxon signed-rank tests on patient-level means. *$*P < 0.05$, **$P < 0.01$, ***$P < 0.001$, ****$P < 0.0001$*; ns, not significant.

Figure S2. CDH3 expression analyzed using published human prostate cancer and breast cancer scRNA-seq datasets.

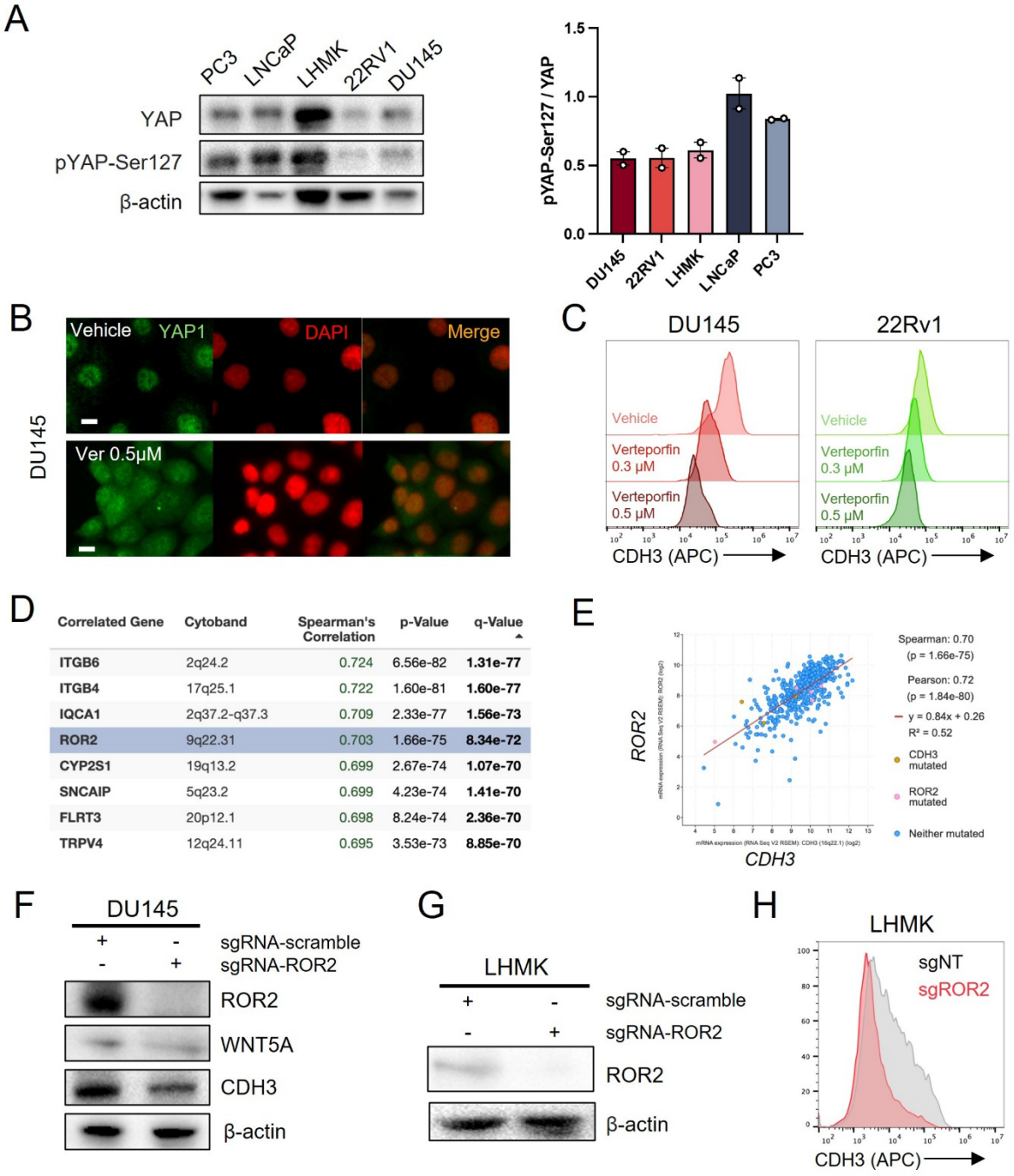




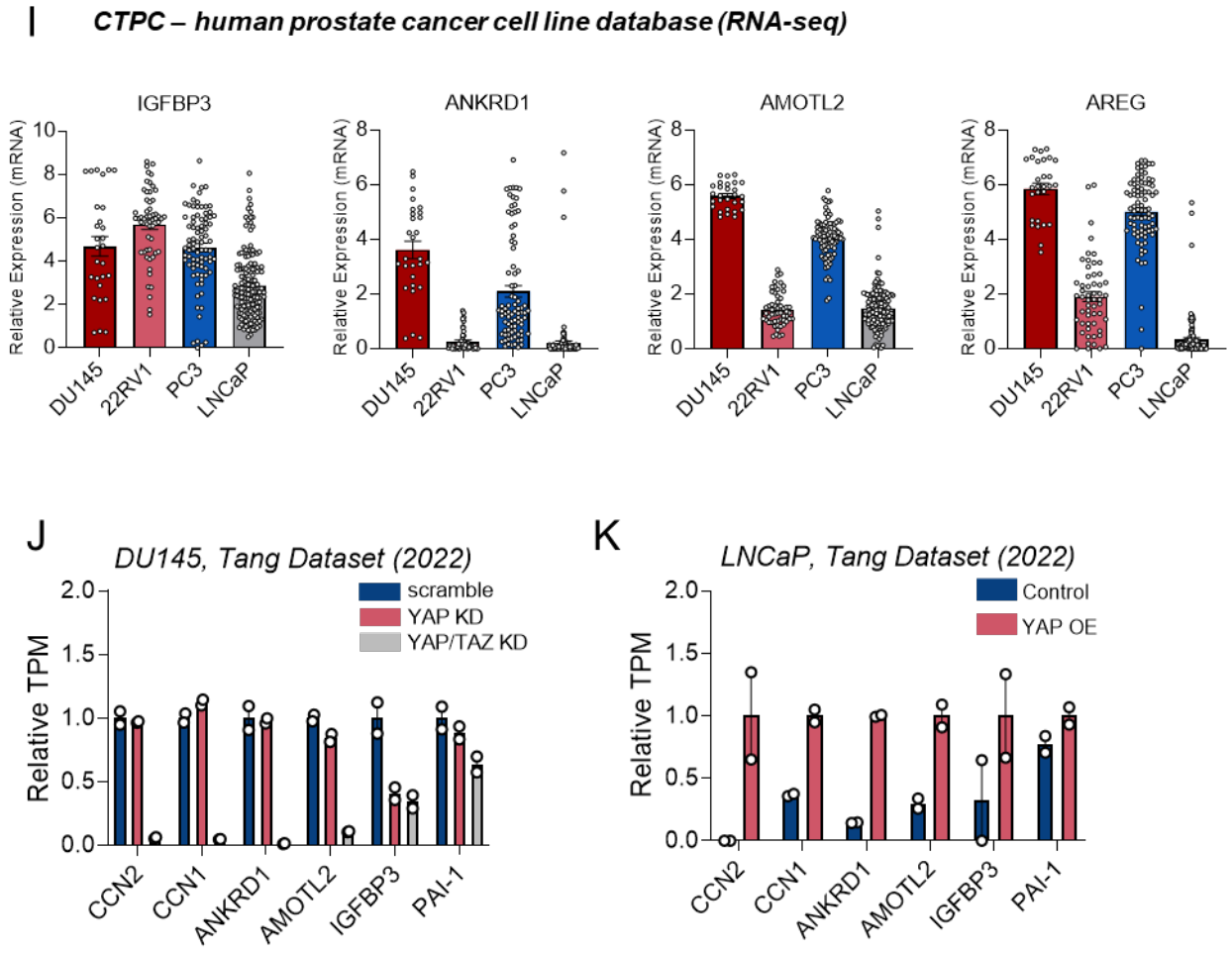
(A) UMAP plots of single-cell RNA-seq data from prostate cancer samples in the Song et al. (2022) dataset, with each panel showing the expression level (purple gradient) of a signature gene. Markers include CDH3, KRT17 (basal epithelial cells), and NKX3-1 (luminal epithelial cells), CD3E (T cells), CD19 (B cells), CCR2/S100A8 (myeloid), NKG7 (NK cells), HLA-DRB1 (antigen-presenting cells), BGN (fibroblasts), CPA3 (mast cells), and VWF (endothelial). Higher intensity (darker purple) indicates stronger expression, facilitating cell-type annotation within the tumor microenvironment. **(B)** Single-cell UMAP for the Wong et al. (2022) dataset showing cells from prostate cancer grouped into basal epithelial, luminal epithelial, immune, and stromal populations. **(C)** CDH3 expression in the epithelial sub-compartment in feature plot (heatmap

scale) and dot plot (dot size indicates percentage of expressing cells; color represents average expression). **(D)** Feature plots for selected non-canonical WNT genes (WNT5A, ROR2) within the epithelial sub-compartment. **(E)** Dot plots showing the average expression (color) and percentage expression (size) of selected canonical and non-canonical WNT pathway components in basal and luminal cancer cells based on Wong dataset. **(F)** Single-cell UMAP for the Jee (2024) dataset showing prostate cancer cells grouped into basal epithelial, luminal epithelial, and neuroendocrine (NE) population. **(G)** CDH3 expression in feature plot (heatmap scale) based on Jee dataset. **(H)** Dot plots showing the average expression (color) and percentage expression (size) of selected canonical and non-canonical WNT pathway components in basal, luminal, and NE prostate cancer cells based on Jee dataset. **(I)** Single-cell UMAP for the Xu et al. (2021) dataset showing breast cancer cells grouped into basal epithelial, luminal epithelial, immune, and stromal populations. **(J)** CDH3 expression in all cells in the feature plot (heatmap scale) and dot plot.

Figure S3. Regulation of CDH3 expression by YAP1 and ROR2.



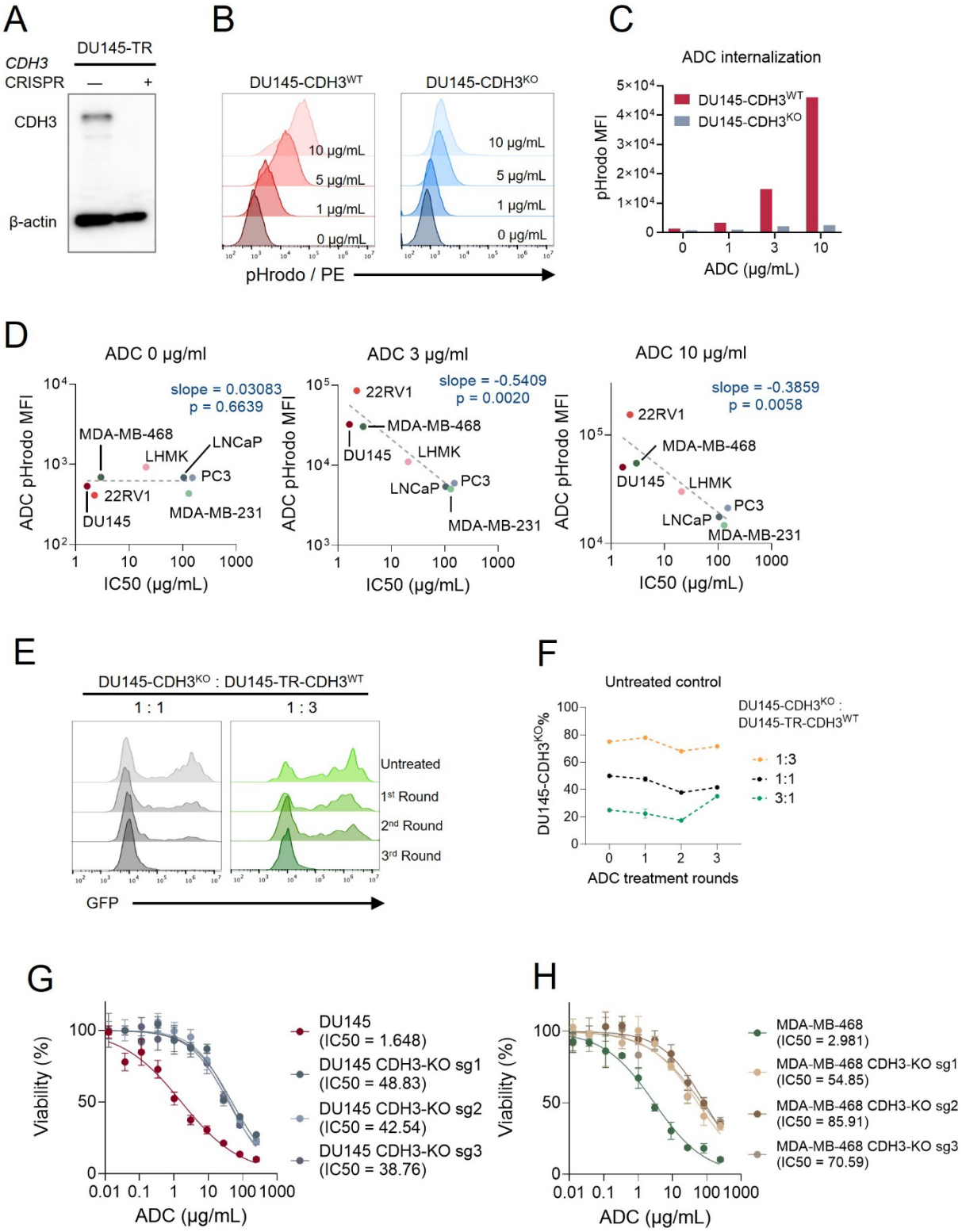
Correlated Gene	Cytoband	Spearman's Correlation	p-Value	q-Value
ITGB6	2q24.2	0.724	6.56e-82	**1.31e-77**
ITGB4	17q25.1	0.722	1.60e-81	**1.60e-77**
IQCA1	2q37.2-q37.3	0.709	2.33e-77	**1.56e-73**
ROR2	9q22.31	0.703	1.66e-75	**8.34e-72**
CYP2S1	19q13.2	0.699	2.67e-74	**1.07e-70**
SNCAIP	5q23.2	0.699	4.23e-74	**1.41e-70**
FLRT3	20p12.1	0.698	8.24e-74	**2.36e-70**
TRPV4	12q24.11	0.695	3.53e-73	**8.85e-70**

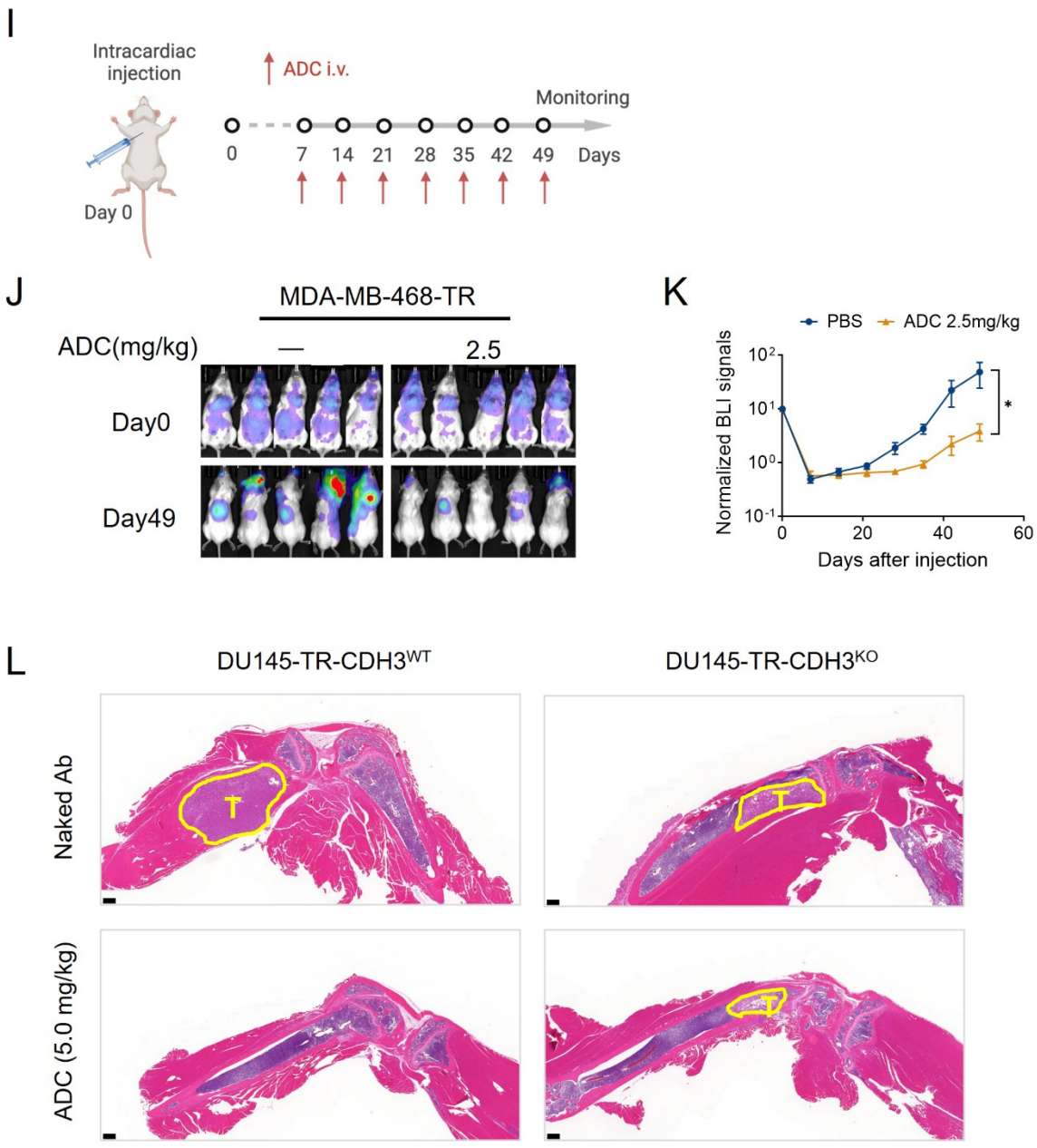


(A) Western blot and semi-quantification of total YAP and phosphorylated YAP (Ser127) in human prostate cancer cell lines. **(B)** Immunofluorescence of YAP1 (green) and nuclei (DAPI, red) in DU145 cells treated with vehicle or verteporfin (Ver) for 72 h. Scale bar, 6 µm. **(C)** Flow cytometry analysis of CDH3 expression in DU145 and 22Rv1 cells treated with vehicle or verteporfin for 72 h. **(D)** Top-ranked genes with *CDH3*-correlated expression in the TCGA PRAD cohort, generated using cBioPortal. **(E)** Scatter plot comparing *CDH3* and *ROR2* transcript levels in the TCGA PRAD cohort, with correlation statistics shown, generated using cBioPortal. **(F)** Western blot of ROR2, WNT5A, CDH3, and β-actin in DU145 sublines stably expressing scramble sgRNA or ROR2-targeted sgRNA. **(G–H)** Western blot confirming ROR2

knockout and flow cytometry analysis of CDH3 expression in LHMK sublines stably expressing scramble sgRNA or ROR2-targeted sgRNA. **(I)** Expression of selected YAP/TAZ-responsive genes across prostate cancer cell lines in the CTPC database, including DU145 (n = 28), 22Rv1 (n = 55), PC3 (n = 84), and LNCaP (n = 148). n denotes the number of independent samples; only wild-type or control samples were included. **(J)** Relative expression of selected YAP/TAZ-responsive genes in DU145 cells following YAP knockdown or YAP/TAZ double knockdown compared with scramble control, reanalyzed from the Tang et al. (2022) RNA-seq dataset. **(K)** Relative expression of selected YAP/TAZ-responsive genes in LNCaP cells following YAP overexpression compared with control, reanalyzed from the Tang et al. (2022) RNA-seq dataset. In **(I-K)**, bars represent mean ± SEM and individual biological replicates are shown.

Figure S4. Effect of CDH3-targeted ADC on prostate cancer and breast cancer cells.

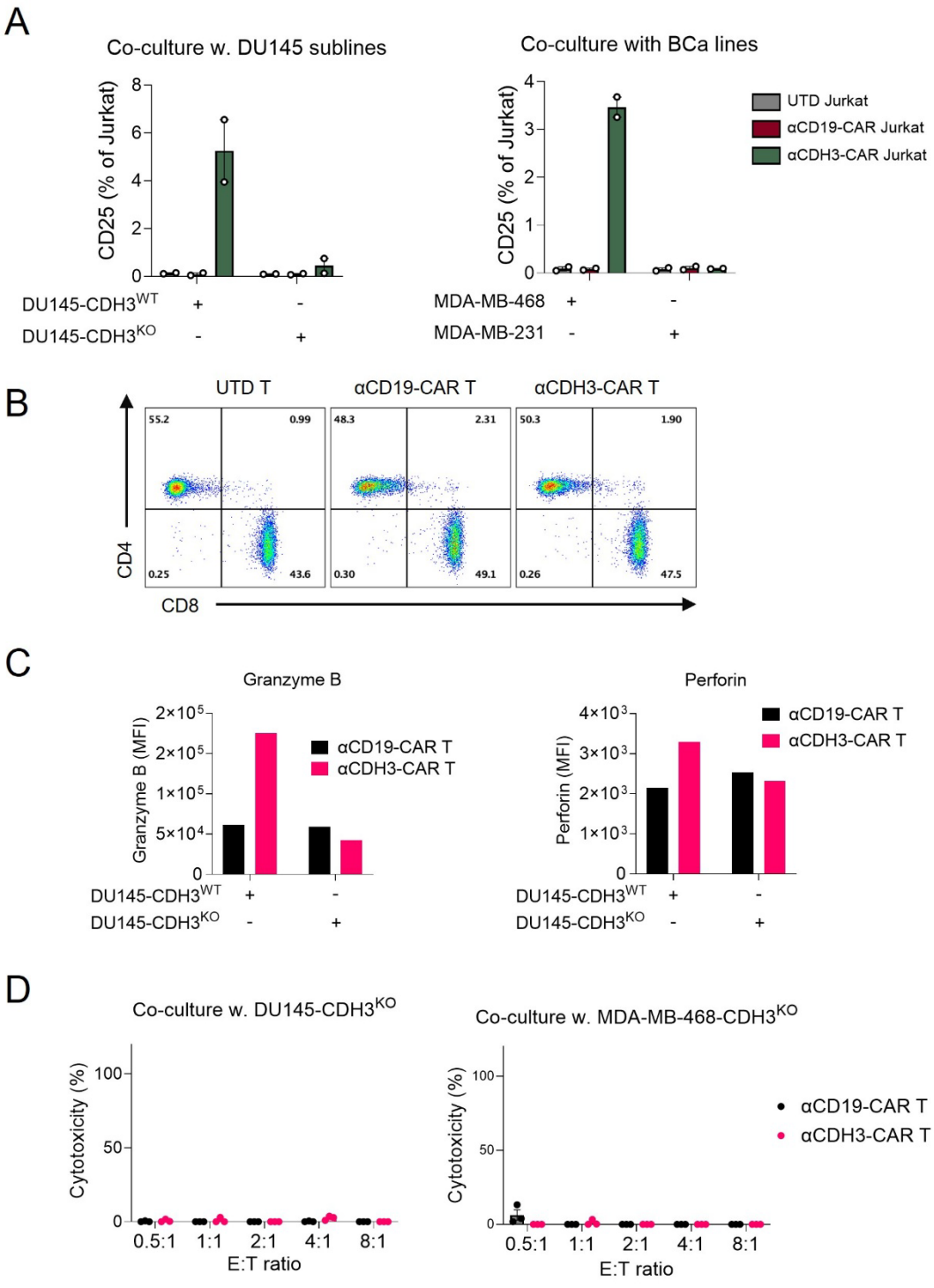




(A) Western blot confirming CDH3 knockout in DU145-TR cells. **(B–C)** Flow cytometric histograms and median fluorescence intensity (MFI) of pHrodo-labeled ADC uptake in DU145-CDH3^{WT} and DU145-CDH3^{KO} cells, measured at different ADC concentrations (0, 1, 5, and 10 µg/mL). **(D)** Correlation between ADC internalization (measured by pHrodo MFI) and cytotoxicity (IC_{50}) in prostate and breast cancer cell lines, with fitted regression slope and significance (p) shown. Each plot corresponds to a different ADC concentration (0, 3, or 10

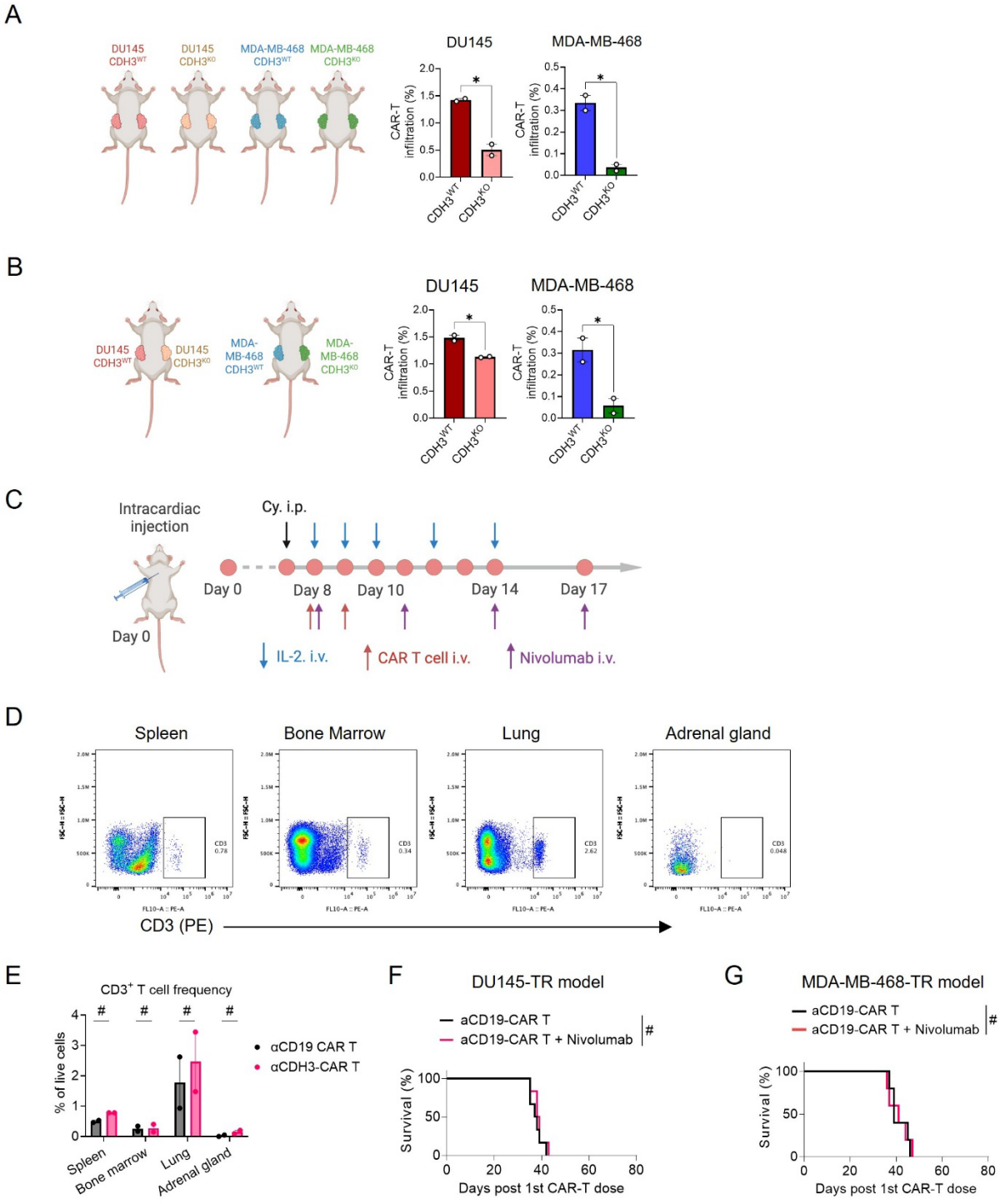
μg/mL). **(E)** Flow cytometric histograms tracking GFP^+ (DU145-TR-$CDH3^{WT}$) and GFP^- (DU145-$CDH3^{KO}$) populations at baseline (untreated) and after each ADC treatment round, shown for 1:1 and 1:3 initial mix ratios. **(F)** Control experiment showing little change in DU145-$CDH3^{KO}$ cell percentages without ADC treatment for the three indicated initial mix ratios. **(G)** Dose-response cytotoxicity curves for DU145 and three DU145-$CDH3^{KO}$ clones (sg1, sg2, sg3) treated with ADC at increasing concentrations (0.01–300 μg/mL). **(H)** Dose-response cytotoxicity curves for MDA-MB-468 and three MDA-MB-468-$CDH3^{KO}$ clones (sg1, sg2, sg3) treated with ADC at increasing concentrations (0.01–300 μg/mL). **(I–K)** Experimental design, representative BLI images (Day 0 and Day 49), hindlimb signal curves (scaled to Day 0 as 10), and endpoint normalized BLI signal for mice intracardiacally injected with MDA-MB-468-TR cells in the absence or presence of ADC treatment (n = 5/group). **(L)** Representative H&E-stained tissue sections from mice bearing DU145-TR-$CDH3^{WT}$ or DU145-TR-$CDH3^{KO}$ tumors treated with naked antibody or anti-CDH3 ADC (5.0 mg/kg). Tissues were collected on day 32 after tumor-cell injection. Tumor areas are outlined in yellow and labeled T. Scale bars, 1 mm. Error bars represent SEM. Extra sum-of-squares F tests were used for **(D)**, and a Mann–Whitney test was used for endpoint normalized BLI signal in **(K)**. $*P < 0.05$.

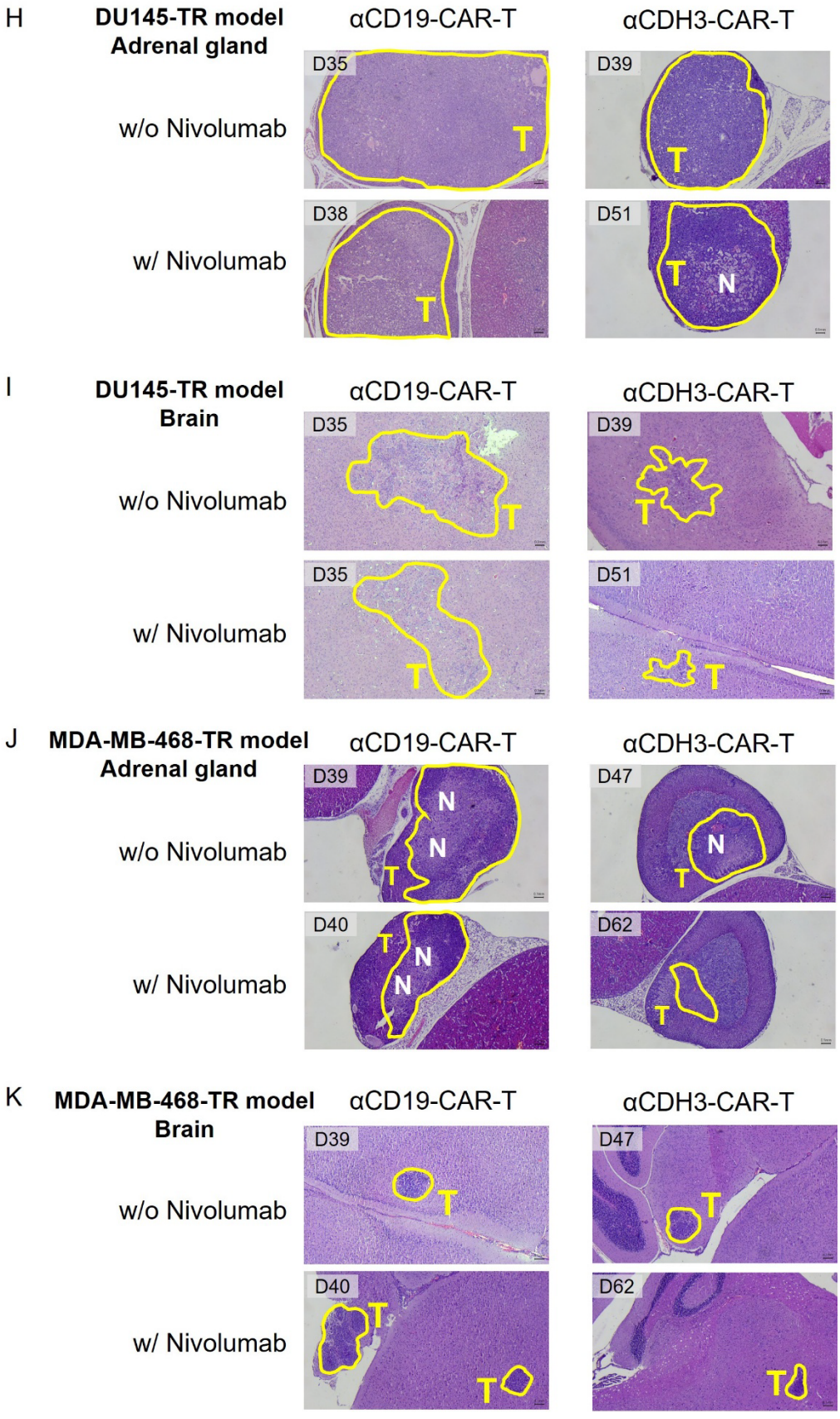
Figure S5. Effect of CDH3-targeted CAR-T cells on prostate cancer and breast cancer cells.



(A) Flow cytometry quantification of activation marker CD25 on Jurkat cells transduced with αCDH3-CAR, αCD19-CAR or untransduced (UTD) and co-cultured with DU145-CDH3^{WT}, DU145-CDH3^{KO} (left panel), MDA-MB-468, or MDA-MB-231 cells (right panel). **(B)** Representative flow cytometry plots showing $CD4^+$ and $CD8^+$ subpopulations in UTD T cells, αCD19-CAR-T cells, or αCDH3-CAR-T cells. **(C)** Median fluorescence intensity (MFI) of granzyme B and perforin in αCD19-CAR-T cells and αCDH3-CAR-T cells after co-culture with DU145-CDH3^{WT} or DU145-CDH3^{KO} cells, measured by flow cytometry. **(D)** Cytotoxicity assays of effector cells (αCD19-CAR-T cells or αCDH3-CAR-T cells) on antigen-absent target cells (DU145-CDH3^{KO} or MDA-MB-468-CDH3^{KO}) at various effector-to-target (E: T) ratios. In **(A)** and **(D)**, error bars represent SEM.

Figure S6. Effect of CDH3-targeted CAR-T cells *in vivo.*

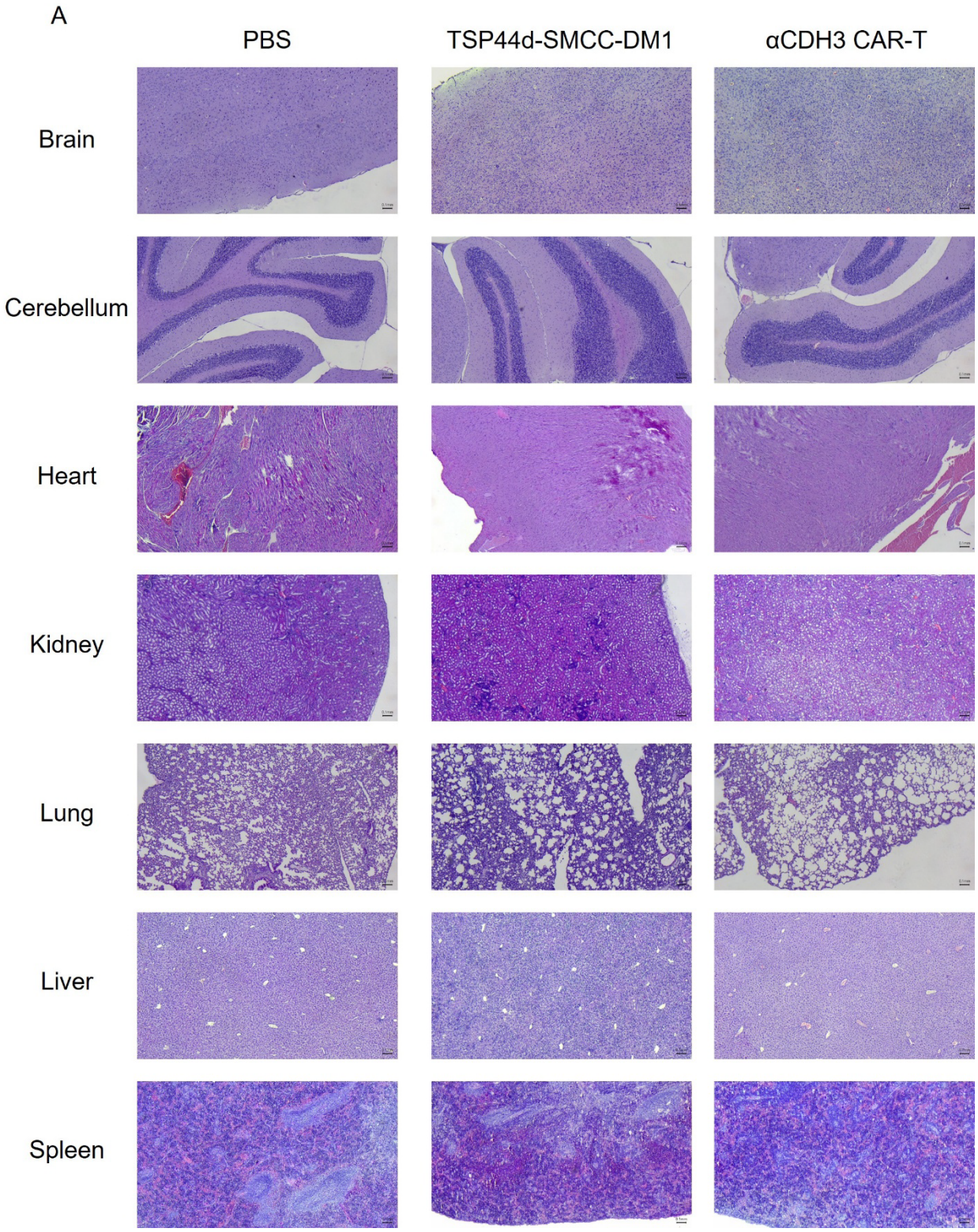



H
DU145-TR model
Adrenal gland
αCD19-CAR-T
αCDH3-CAR-T
w/o Nivolumab
w/ Nivolumab
D35
D39
D38
D51
T
N
I
DU145-TR model
Brain
αCD19-CAR-T
αCDH3-CAR-T
w/o Nivolumab
w/ Nivolumab
D35
D39
D35
D51
T
J
MDA-MB-468-TR model
Adrenal gland
αCD19-CAR-T
αCDH3-CAR-T
w/o Nivolumab
w/ Nivolumab
D39
D47
D40
D62
N
T
K
MDA-MB-468-TR model
Brain
αCD19-CAR-T
αCDH3-CAR-T
w/o Nivolumab
w/ Nivolumab
D39
D47
D40
D62
T

(A) Experimental design of single subline per mouse and quantification of αCDH3-CAR T cell infiltration into subcutaneous tumors formed by two DU145 sublines in male NOD/SCID mice or two MDA-MB-468 sublines in female NOD/SCID mice, 7 days after T cell infusion. **(B)** Experimental design of paired sublines per mouse and quantification of αCDH3-CAR T cell infiltration into subcutaneous tumors formed by two DU145 sublines in male NOD/SCID mice or two MDA-MB-468 sublines in female NOD/SCID mice, 7 days after T cell infusion. **(C)** Experimental design showing the timing of CAR-T therapy in the metastatic model. DU145-TR cells were delivered via intracardiac injection on Day 0, followed by cyclophosphamide (Cy) administered intraperitoneally for lymphodepletion and repeated IL-2 treatment to support CAR-T therapy, given alone or in combination with nivolumab. **(D–E)** Representative flow cytometry dot plots and quantification of αCD19-CAR or αCDH3-CAR T cell frequencies in four organs 1 day after CAR-T infusion in NOD/SCID mice bearing DU145-TR metastases. **(F)** Survival curves for mice bearing DU145-TR metastases and treated with αCD19-CAR T + control (n = 6) or αCD19-CAR T + nivolumab (n = 6). **(G)** Survival curves for mice bearing MDA-MB-468-TR metastases and treated with αCD19-CAR T + control (n = 5) or αCD19-CAR T + nivolumab (n = 5). **(H–I)** Representative H&E-stained sections of adrenal glands and brains, respectively, from mice bearing DU145-TR metastases following treatment with αCD19-CAR T or αCDH3-CAR T cells, with or without nivolumab. **(J–K)** Representative H&E-stained sections of adrenal glands and brains, respectively, from mice bearing MDA-MB-468-TR metastases following treatment with αCD19-CAR T or αCDH3-CAR T cells, with or without nivolumab. Day labels indicate the time of tissue collection after the first CAR-T dose. Tumor areas are outlined in yellow and labeled T; necrotic areas are labeled N. Scale bars, 0.1 mm.

In **(A)**, **(B)**, and **(E)**, error bars represent SEM. Unpaired t tests were used for **(A)**, **(B)**, and **(E)**, and log-rank (Mantel–Cox) tests were used for **(F)** and **(G)**. *$P < 0.05$; #, not significant.

Figure S7. Histological assessment of major organs following CDH3-directed ADC or CAR-T treatment



(A) Representative H&E-stained sections of brain, cerebellum, heart, kidney, lung, liver, and spleen collected from mice treated with PBS, TSP44d-SMCC-DM1 ADC, or αCDH3 CAR-T cells. N=3 per group. Scale bars, 0.1 mm.

Table S1. Software packages used in the bioinformatic analysis

Package	Version	Software
biomaRt	2.58.2	R
Msigdbr	7.5.1	R
Limma	3.58.1	R
consensusclusterplus	1.66	R
GSVA	1.5	R
EdgeR	4.0.12	R
ggplot2	3.5.1	R
pheatmap	1.0.12	R
ComplexHeatmap	2.18	R
Seurat	5.0.1	R
scType	Github	R
SingleR	2.4.1	R
ggalluvial	0.12.5	R
singscore	1.30.0	R

Table S2. Antibodies used in this study

Target	Isotype	Conjugate	Clone	Source	Cat#	Experiment
Human CDH3	Human IgG	-	TSP44d	Custom antibody developed by Perseus Proteomics		Therapy, flow cytometry
YAP1	Rabbit IgG	-	D8H1X	Cell Signaling Technology	14074	IF, WB
pYAP1-Ser127	Rabbit IgG	-	D9W2I	Cell Signaling Technology	13008	WB
ROR2	Rabbit IgG	-	D3B6F	Cell Signaling Technology	88639	WB
Human CDH3	Mouse IgG	-	12H6	Cell Signaling Technology	14029	WB
Human/Mouse Wnt5a	Rat IgG	-	442625	R&D System	MAB645	WB
β-actin	Mouse IgG	-	C4	Santa Cruz	sc-47778	WB
α-tubulin	Mouse IgG	-	B-7	Santa Cruz	sc-5286	WB
Human CD45	Mouse IgG	PE	HI30	BD	560975	Flow cytometry
Human CD3	Mouse IgG	APC	UCHT1	BD	561810	Flow cytometry
Human CD4	Mouse IgG	APC/Cyanine7	RPA-T4	BioLegend	300518	Flow cytometry
Human CD8	Mouse IgG	PE	SK1	BioLegend	344706	Flow cytometry
Human CD25	Mouse IgG	PE	BC96	Cytek	50-0259	Flow cytometry
Human CD69	Mouse IgG	APC	FN50	Cytek	20-0699	Flow cytometry
Human CD45RO	Mouse IgG	APC	UCHL1	BioLegend	983102	Flow cytometry
Human CD62L	Mouse IgG	PerCP/Cyanine5.5	DREG-56	BioLegend	304824	Flow cytometry
Human/Mouse Granzyme B	Mouse IgG	PE/Cyanine7	QA16A02	BioLegend	372214	Flow cytometry
Human Perforin	Mouse IgG	PerCP/Cyanine5.5	B-D48	BioLegend	353313	Flow cytometry
Human IgG	Goat IgG	AF647	Polyclonal	Jackson ImmunoResearch	109-605-088	Flow cytometry
Rabbit IgG	Goat IgG	AF647	Polyclonal	Jackson ImmunoResearch	711-605-152	IF
Human PD-1 (Nivolumab)	Human IgG	-	5C4	Leinco	LT1200	Therapy

Table S3. Public datasets used in this study

Dataset	Year	Description	Public Access
Tang Dataset	2022	Bulk RNA-seq of CRPC cell lines, organoids and PDXs	GSE199190
CTPC	2023	Combined transcriptomic dataset of human prostate cancer cell lines	CTPC online platform
Mayo Clinic	2014	Bulk microarray of patient prostate cancer	GSE46691
Cleveland Clinic	2014	Bulk microarray of patient prostate cancer	GSE62267
Thomas Jefferson Hospital	2016	Bulk microarray of patient prostate cancer	GSE72291
Johns Hopkins Hospital	2016	Bulk microarray of patient prostate cancer	GSE79958
TCGA PRAD	-	Bulk RNA-seq of patient primary prostate cancer	cBioportal
TCGA BRCA	-	Bulk RNA-seq of patient primary breast cancer	cBioportal
SU2C mCRPC	2019	Bulk RNA-seq and clinical data from mCRPC	cBioportal
Fred Hutch Cancer Center	-	Transcriptomics of patient primary and metastasis prostate cancer	cBioportal
AURORA	2023	Bulk RNA-seq of normal, primary, and metastatic breast specimens	GSE193103
Song Dataset	2022	Single-cell RNA-seq of prostate cancer	GSE176031
Wong Dataset	2022	Single-cell RNA-seq of prostate cancer	GSE185344
Jee Dataset	2024	Single-cell RNA-seq of prostate cancer	GSE221603
Jin Dataset	2024	Single-cell RNA-seq of breast cancer	GSE263995
Xu Dataset	2021	Single-cell RNA-seq of breast cancer	GSE180286